# Code-division-multiplexed readout of large arrays of TES microcalorimeters

K. M. Morgan, B. K. Alpert, D. A. Bennett, E. V. Denison, W. B. Doriese, J. W. Fowler, J. D. Gard, G. C. Hilton, K. D. Irwin, Y. I. Joe, G. C. O'Neil, C. D. Reintsema, D. R. Schmidt, J. N. Ullom, and D. S. Swetz

Citation: Appl. Phys. Lett. **109**, 112604 (2016);

View online: https://doi.org/10.1063/1.4962636

View Table of Contents: http://aip.scitation.org/toc/apl/109/11

Published by the American Institute of Physics

# Code-division-multiplexed readout of large arrays of TES microcalorimeters

K. M. Morgan,[1,a)] B. K. Alpert,[1] D. A. Bennett,[1] E. V. Denison,[1] W. B. Doriese,[1] J. W. Fowler,[1] J. D. Gard,[1] G. C. Hilton,[1] K. D. Irwin,[2] Y. I. Joe,[1] G. C. O'Neil,[1] C. D. Reintsema,[1] D. R. Schmidt,[1] J. N. Ullom,[1] and D. S. Swetz[1,b)]
[1]*National Institute of Standards and Technology, Boulder, Colorado 80305, USA*
[2]*Stanford University, Palo Alto, California 94305, USA*

(Received 28 July 2016; accepted 27 August 2016; published online 15 September 2016)

Code-division multiplexing (CDM) offers a path to reading out large arrays of transition edge sensor (TES) X-ray microcalorimeters with excellent energy and timing resolution. We demonstrate the readout of X-ray TESs with a 32-channel flux-summed code-division multiplexing circuit based on superconducting quantum interference device (SQUID) amplifiers. The best detector has energy resolution of $2.28 \pm 0.12$ eV FWHM at 5.9 keV and the array has mean energy resolution of $2.77 \pm 0.02$ eV over 30 working sensors. The readout channels are sampled sequentially at 160 ns/row, for an effective sampling rate of 5.12 $\mu$s/channel. The SQUID amplifiers have a measured flux noise of 0.17 $\mu\Phi_0/\sqrt{\text{Hz}}$ (non-multiplexed, referred to the first stage SQUID). The multiplexed noise level and signal slew rate are sufficient to allow readout of more than 40 pixels per column, making CDM compatible with requirements outlined for future space missions. Additionally, because the modulated data from the 32 SQUID readout channels provide information on each X-ray event at the row rate, our CDM architecture allows determination of the arrival time of an X-ray event to within 275 ns FWHM with potential benefits in experiments that require detection of near-coincident events. *Published by AIP Publishing.* [http://dx.doi.org/10.1063/1.4962636]

A transition-edge sensor (TES) microcalorimeter is a superconducting thin film in which the superconducting-to-normal transition is used to measure the energy of individual X-ray photons to very high precision. Single-pixel TES detectors can now achieve resolving powers of 2000–4000 in the 1–10 keV energy range.[1–3] TES arrays provide a compact spectrometer geometry and orders-of-magnitude improvement in efficiency/throughput versus traditional wavelength-dispersive instruments.[4] This has made the TES spectrometer an attractive candidate technology for the next generation of astronomical X-ray observatories,[5,6] neutrino mass experiments,[7] measurements of X-ray fundamental parameters,[8] and table top and facility-scale light sources.[9] To date, readout of X-ray TESs has been limited to hundreds of pixels per array.[10] Future spectrometers call for several kilopixels, or even hundreds of kilopixels,[5,6] which will require new techniques for reading out large numbers of sensors.

State-of-the-art readout systems for hundreds of TES microcalorimeters employ time-division multiplexing (TDM).[11] In a typical TDM system, a single readout column consists of $N$ rows of TESs, each coupled to a superconducting quantum interference device (SQUID) amplifier. Rows are turned on and read out in succession. As the number of detectors per column increases, the effective sampling rate per sensor (frame rate) decreases. Additionally, the SQUID noise aliased into the signal band grows[12] as $\sqrt{N_{\text{rows}}}$. Another technique being developed for X-ray TES readout is frequency-division multiplexing (FDM), which places TESs in series with $LC$ resonant circuits and ac biases the sensors at different MHz frequencies. FDM avoids the $\sqrt{N}$ noise penalty and samples all sensors in a column simultaneously. However, the $LC$ components can be physically large[30] and studies have shown degraded sensor resolution under ac bias, though it is not currently known if this is inherent to the technique.[13] Another alternative scheme is the microwave-SQUID multiplexer ($\mu$MUX) in which high-$Q$ superconducting microwave resonators are coupled to rf SQUIDs and read out on a common feedline through a high-bandwidth HEMT amplifier.[14] Though initial two-pixel demonstrations look promising, $\mu$MUX readout is still in the very early stages of development.[15]

Our team has previously demonstrated the readout of eight X-ray TESs via flux-summed code-division multiplexing ($\Phi$-CDM).[16] In this letter, we describe the readout of an array of TESs with a 32-channel $\Phi$-CDM circuit. The mean energy resolution is $2.77 \pm 0.02$ eV FWHM at 5.9 keV for 30 modulated sensors. With a redesigned multiplexer chip and fast data-acquisition electronics, we show that the readout noise and bandwidth of this system can meet the needs of the next generation of X-ray space missions, providing a clear path to kilopixel-scale arrays of TESs. Finally, we demonstrate that the modulated data stream can be used to determine the photon-arrival time to significantly better than one readout frame.

In CDM, the signals from the TESs are encoded with a Walsh basis set[17] such that during each time step the signals from all dc-biased TESs in a readout column are summed with equal weight but different polarity patterns.[18,19] In the flux-summing architecture used here, we accomplish this encoding by passively summing the current signals from the $N$ different microcalorimeters in $N$ different SQUIDs with different combinations of coupling polarities (more details can be found in Stiehl *et al.*[16]). The SQUIDs are then read out in sequence at the row time ($t_{\text{row}}$). The feedback that is

a)Electronic mail: kelsey.morgan@nist.gov
b)Electronic mail: swetz@nist.gov

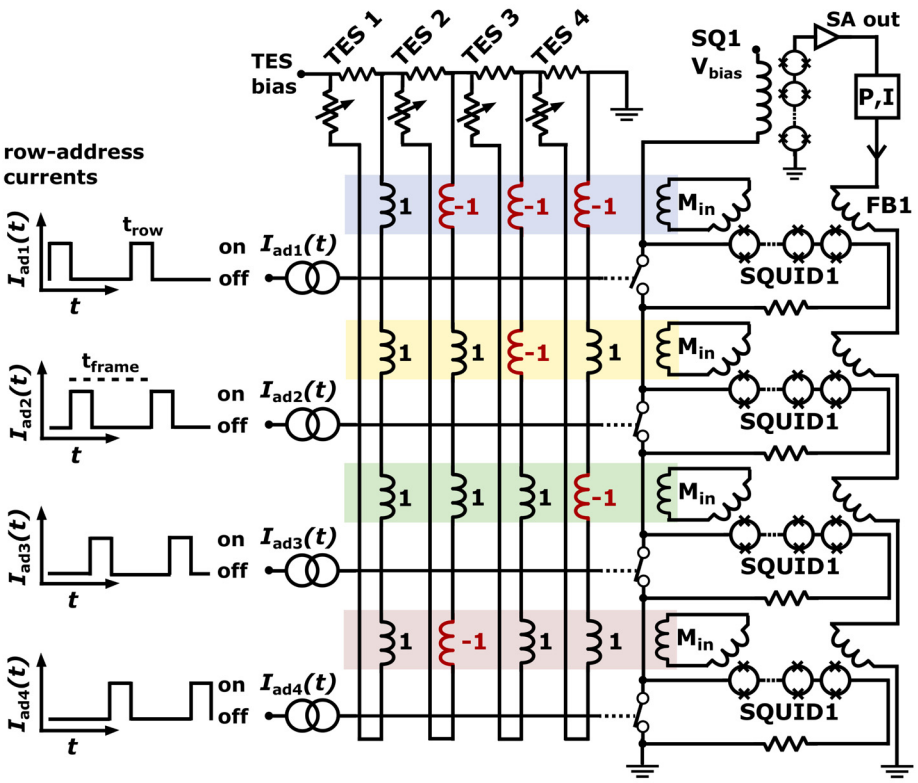


FIG. 1. A 4-channel example of a CDM circuit. Bias to each SQUID channel is controlled by applying address current ($I_{ad}$) to a flux-actuated switch. A common feedback signal (FB1) is applied to all channels. Current signals from each TES are coupled positively or negatively to each SQUID channel.

applied to linearize the signal for a single SQUID channel is applied only once per frame ($Nt_{row}$) as in TDM. However, unlike in TDM all TESs are sampled at every row switch. Once decoded, the TES signals average coherently while the amplifier noise averages incoherently, eliminating the $\sqrt{N}$ noise penalty.[16]

The schematic in Fig. 1 shows four of the 32 SQUID channels on our Φ-CDM chip. Each SQUID channel consists of a 6-SQUID series array that is coupled either positively or negatively to each of the 32 TESs according to the requirement of the Walsh encoding. The SQUID channels are read out sequentially by modulation of their biases on and off with flux-actuated switches, an architecture first suggested by Zappe.[20] The overall system bandwidth is $f_{OL} \approx 6$ MHz, allowing the row switching time to be as short as 160 ns. The signals from the 32 SQUID channels are then sent sequentially to a SQUID series array, and finally to a room-temperature preamplifier.

To reconstruct events, the raw data must be demodulated by multiplication of the $N$ channels of data produced by the Φ-CDM system by the $N \times N$ inverse Walsh matrix ($W_N^{-1}$) containing the coupling coefficients for each sensor to each SQUID input (Fig. S1 in the supplementary material). Departures from integer coupling ($\pm 1$) are observed on the order of a few percent due to minor differences in coil geometries across TES channels inherent in the chip architecture, as well as various on-chip sources of crosstalk. This causes spurious signals to appear in demodulated data streams for TESs that did not observe an X-ray event. A correction to the integer $W_N$ matrix can be computed[21] to reduce this effect to levels below 0.1%.

Fig. 2 shows a Mn Kα (5.9 keV) fluorescence spectrum measured by 30 TES sensors read out through our 32-channel Φ-CDM circuit. The TESs are $350\,\mu m \times 350\,\mu m$ Mo/Cu bilayers with a 2.5 μm thick bismuth layer added to increase efficiency.[22] Under the bias and magnetic field conditions used for this demonstration, the sensors have an average inherent resolution of 2.7 eV, with significant pixel-to-pixel variation. Though 32 sensors were bonded to the CDM chip, one of these became an open circuit during cooldown. The construction of the Walsh matrix for encoding requires one TES to remain unswitched, that is, it couples to all SQUID inputs in the same direction. In the switched TESs, any sources of noise (such as pickup of noise sources or gain variations in amplifier elements) that enter the amplifier chain after the switched

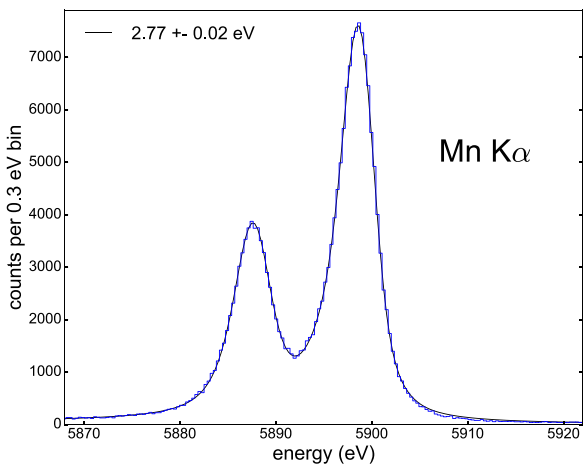


FIG. 2. Mn Kα X-ray fluorescence spectrum measured by 30 TESs read out by 32-channel Φ-CDM. The source produced approximately 0.3 counts per second per TES. The data are well-fit by the intrinsic Mn Kα line shape[23] with Gaussian broadening due to the energy resolution of the TESs of $2.77 \pm 0.02$ eV FWHM.

elements and are slower the frame rate will be canceled coherently during demodulation. The unswitched TES does not benefit from this effect and thus sees increased low frequency noise which degrades its resolution to $3.65 \pm 0.12$ eV FWHM. Combining the spectra of the remaining 30 pixels, the array achieves energy resolution of $2.77 \pm 0.02$ eV FWHM at 5.9 keV. The best single pixel measured had a multiplexed resolution of $2.28 \pm 0.12$ eV FWHM.

In this CDM chip we measured single-channel flux noise of $0.15\,\mu\Phi_0/\sqrt{\text{Hz}}$. Including contributions from the rest of the amplifier chain, the total single-channel noise is $0.17\,\mu\Phi_0/\sqrt{\text{Hz}}$. Since the SQUID noise contribution (referred to the TES) does not increase with $N_{\text{rows}}$ in CDM, we are able to reduce the input coupling to the sensors by a factor of 6 versus our standard TDM readouts without the amplifier noise significantly degrading the sensors' energy resolution. The lower input coupling also reduces the maximum flux slew rate observed during a pulse, which in turn allows more sensors per column for a fixed readout bandwidth.

The measured amplifier noise and switching speed for this system can be scaled to determine the viability of Φ-CDM as a readout architecture for kilopixel-scale arrays. As a case study, we consider the specifications for the X-ray integral field unit (X-IFU) instrument being designed for the Athena X-ray satellite mission. The X-IFU specification requires energy resolution better than 2.5 eV at 6 keV, and in the most recent implementation the multiplexer reads out 40 pixels per column.[5] To model the TES response, we use the canonical detector model developed for the International X-ray Observatory (IXO).[24] To meet the energy resolution requirement with 40 rows per column, the TES-current-referenced multiplexed SQUID noise ($\sqrt{S_{\text{I}_{\text{MUX}}}}$) should be less than about $45\,\text{pA}/\sqrt{\text{Hz}}$.[25] For CDM, the relation between the maximum allowed multiplexed SQUID noise and the non-multiplexed single-channel SQUID noise ($\sqrt{S_\Phi}$) is[18]

$$M_{\text{in}}\sqrt{S_{\text{I}_{\text{MUX}}}} \geq \sqrt{\pi S_\Phi}, \tag{1}$$

where $M_{\text{in}}$ is the first-stage SQUID input mutual inductance. The maximum TES current slew rate sets the longest acceptable frame time. The SQUID output current must remain linear with input flux during operation as a flux-locked loop. This constraint can be expressed as

$$\Delta\Phi_{\text{max}} = \left.\frac{dI}{dt}\right|_{\text{max}} M_{\text{in}} N_{\text{rows}} t_{\text{row}} \leq X\Phi_0/2, \tag{2}$$

where $\left.\frac{dI}{dt}\right|_{\text{max}}$ is the maximum TES current slew rate during a pulse and $X$ is the fraction of a $\Phi_0$ over which the SQUID output current remains linear. The available linear range is reduced by a factor of 2 in CDM because pulses are both upward- and downward-going. For the IXO-like detector model, $\left.\frac{dI}{dt}\right|_{\text{max}}$ may be up to 1 A/s. For our CDM circuit, $X \approx 1/5$. Combining Eqs. (1) and (2) gives a constraint on the product of $t_{\text{row}}$ and non-multiplexed SQUID noise

$$t_{\text{row}}\sqrt{S_\Phi} \leq \frac{X\Phi_0}{2N_{\text{rows}}}\left(\left.\frac{dI}{dt}\right|_{\text{max}}\right)^{-1}\sqrt{\frac{S_{\text{I}_{\text{MUX}}}}{\pi}}. \tag{3}$$

A similar expression for CDM readout is derived by Doriese *et al.* in 2012;[25] however, due to a typographical error that work incorrectly reports a dependence on $1/\sqrt{N_{\text{rows}}}$ rather than $1/N_{\text{rows}}$. Figure 3 (blue line) plots the constraint in Eq. (3) on $\sqrt{S_\Phi}$ and $t_{\text{row}}$ for the IXO-like TES model assuming 40 readout rows per column and 2.5 eV desired energy resolution (including degradation due to amplifier noise). The non-multiplexed SQUID noise ($0.17\,\mu\Phi_0/\sqrt{\text{Hz}}$) and readout rate (160 ns) in our current CDM system meet these constraints with significant engineering margin. Since noise does not increase with number of rows, the SQUID input coupling ($M_{\text{in}}$) can be reduced by $\sqrt{N_{\text{rows}}}/2$ relative to a TDM system while maintaining the same noise performance to expand the available dynamic range (Fig. S2 in the supplementary material). Adjusting $M_{\text{in}}$ would allow, in principle, multiplexing up to 92 sensors in a single readout column while still meeting speed and noise requirements. Alternatively, the performance margin provided by CDM could be used to multiplex sensors with better inherent energy resolution or higher current slew rates.

An additional feature of CDM is that all TESs are sampled in every row, unlike in TDM where each TES is sampled only once per frame. Therefore, in CDM information about the photon arrival time can be derived from the modulated data stream to achieve sub-frame arrival time resolution. Precise determination of arrival time is of interest in many experiments that must detect coincident events. For example, arrival time may be used to distinguish signal from background in experiments with a triggered signal and a random calibration source.[7,8,27,28]

We can determine photon arrival time by examining the modulated signals in all 32 SQUID channels (which are sampled sequentially at $t_{\text{row}}$) to identify the time at which the current signal in any SQUID channel ($I_{\text{N}}$) starts to deviate from the baseline. When an X-ray arrives, the derivative of

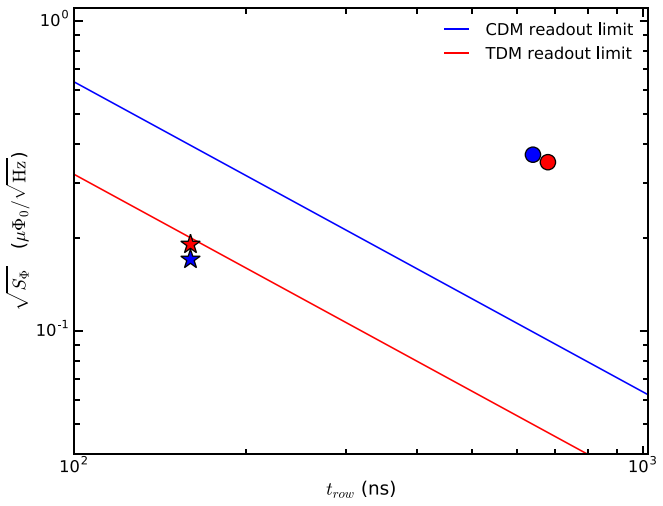


FIG. 3. The plot shows constraints on SQUID noise and row time for 40-row multiplexed readout of Athena-like TESs. The area below the blue line shows allowed combinations of $t_{\text{row}}$ and $\sqrt{S_\Phi}$ for CDM. The farther points lie below the line, the more engineering margin is available. The red line shows the same constraint for TDM, where $t_{\text{row}}\sqrt{S_\Phi} \leq \Phi_0\left(\left.\frac{dI}{dt}\right|_{\text{max}}\right)^{-1}\left(S_{\text{I}_{\text{MUX}}}/\pi^3 N_{\text{rows}}^3\right)^{\frac{1}{2}}$ due to the $\sqrt{N_{\text{rows}}}$ noise penalty.[25] The model assumes a maximum TES signal slew rate of 1 A/s and total multiplexed amplifier noise $\sqrt{S_{\text{I}_{\text{MUX}}}} = 45\,\text{pA}/\sqrt{\text{Hz}}$ referred to the TES. The CDM readout described in this letter is shown by the blue star. A previous 8-row CDM demonstration is shown as a blue circle.[16] Also shown are demonstrations of 32-row[11] (red star) and 8-row[26] (red circle) TDM readout.

$I_N$ increases sharply due to the large slew rates on the rising edge of a pulse. For each SQUID channel, we compute the derivative $\Delta I_N$ at the $i$-th sample in a digitized event record using 4 successive samples of that channel, each separated in time by $t_{frame} = 32t_{row}$

$$\Delta I_{N,i} = ((I_{N,i+1} + I_{N,i}) - (I_{N,i-1} + I_{N,i-2}))/4t_{frame}. \quad (4)$$

We repeat this process for all 32 channels, multiplying $I_N$ by $-1$ where appropriate to account for channels with negative coupling polarities. We then combine the data by offsetting each $\Delta I_N$ in time by $Nt_{row}$. Fig. 4 shows $\Delta I_N$ as a function of time for 32 channels within two frames containing the arrival of an X-ray. By fitting a model consisting of a flat baseline and a linear rise, we determine the point at which the slope of $\Delta I_N$ is no longer zero and assign this point to be the arrival time of the photon.

We applied this method to 10 000 Mn Kα fluorescence events with randomly distributed arrival times from all 31 working TESs. First, we fit the data with two free parameters: the slope of the linear rise and the location of the "knee" that represents arrival time. Because the Mn Kα complex is confined to a narrow energy range, all pulses have a similar rising edge and we can fix the slope of the linear rise to the mean value from the initial fit. We then re-fit the data with the arrival time as the only free parameter. Using this iterative method we find that the arrival times are uniformly distributed within a frame, as expected for events that arrive at random (see Fig. 4 inset). We estimate the time resolution we achieve using the mean uncertainty on the fitted arrival times. This error is 275 ns FWHM, a factor of 19 times more precise than the 5.12 μs frame time. Because the time resolution depends on the signal-to-noise ratio of the system it could be improved in future systems by increasing the coupling between the SQUID amplifiers and the TESs.

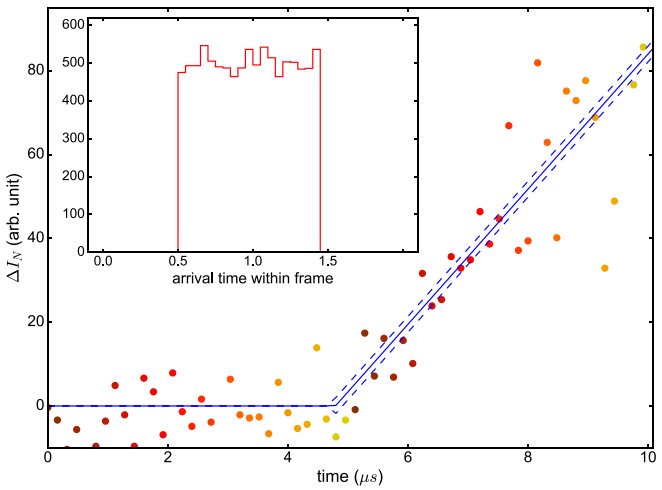


FIG. 4. Arrival time is determined by computing the derivative of the SQUID current $\Delta I_N$ in all 32 channels for two readout frames encapsulating a photon arrival, then fitting a model (blue line) consisting of a flat baseline plus a line with fixed slope. The "knee" in the fit is taken as the arrival time. The plot shows $\Delta I_N$ for two frames of data from the 32 SQUID channels combined for a single X-ray event. The signal from each SQUID channel is represented by a different colored point. 1-$\sigma$ error bars on the best fit are shown as dashed lines. The inset shows the distribution of arrival times for 10 000 events.

For broadband data, an X-ray source with multiple known energies could be used to build up a calibration curve consisting of the slope of the linear ramp as a function of energy, similar to the energy calibration curves used for microcalorimeter data.[29] Without using this iterative fitting process to fix the slope, our estimate of the arrival time uncertainty is 380 ns FWHM.

In summary, we built a 32-channel flux-summed code-division multiplexing chip and used it to read out 30 TESs with 2.77 eV FWHM combined resolution at 5.9 keV. The modulated data can be used to determine photon arrival time to within 275 ns FWHM. The Φ-CDM chips are also "drop-in compatible" with our existing TDM systems, including SQUID series arrays, room temperature electronics, and data acquisition systems. The noise performance and readout speed achieved provide large margins for increasing the number of rows per column and reading out faster sensors without significantly degrading their energy resolution. This flexibility makes CDM an excellent candidate for future applications requiring large arrays of microcalorimeters.

See supplementary material for an example of signal demodulation and details regarding the voltage-flux characteristics and available linear range of the SQUID amplifiers used in the CDM circuit.

We gratefully acknowledge financial support from the NIST Innovations in Measurement Science Program and NASA through the Grant Nos. NNG16PT18I and NNH11ZDA001N-SAT. This work is supported by a National Research Council Post-Doctoral Fellowship. We thank the X-ray Microcalorimeter group at NASA Goddard Space Flight Center for useful discussions and advice. Contribution of NIST, not subject to copyright.

[1]S. J. Lee, J. S. Adams, S. R. Bandler, J. A. Chervenak, M. E. Eckart, F. M. Finkbeiner, R. L. Kelley, C. A. Kilbourne, F. S. Porter *et al.*, Appl. Phys. Lett. **107**, 223503 (2015).
[2]S. J. Smith, J. S. Adams, C. N. Bailey, S. R. Bandler, J. A. Chervenak, M. E. Eckart, F. M. Finkbeiner, R. L. Kelley, C. A. Kilbourne *et al.*, J. Low Temp. Phys. **167**, 168 (2012).
[3]J. W. Fowler, B. K. Alpert, W. B. Doriese, D. A. Fischer, C. Jaye, Y. I. Joe, G. C. O'Neil, D. S. Swetz, and J. N. Ullom, Astrophys. J. Suppl. Ser. **219**, 35 (2015).
[4]J. Uhlig, W. B. Doriese, J. W. Fowler, D. S. Swetz, C. Jaye, D. A. Fischer, C. D. Reintsema, D. A. Bennett, L. R. Vale, U. Mandal *et al.*, J. Synchrotron Radiat. **22**, 766 (2015).
[5]L. Ravera, D. Barret, J. W. den Herder, L. Piro, R. Clédassou, E. Pointecouteau, P. Peille, F. Pajot, M. Arnaud, C. Pigot *et al.*, Proc. SPIE **9144**, 91442L (2014).
[6]J. A. Gaskin, M. C. Weisskopf, A. Vikhlinin, H. D. Tananbaum, S. R. Bandler, M. W. Bautz, D. N. Burrows, A. D. Falcone, F. A. Harrison, R. K. Heilmann *et al.*, Proc. SPIE **9601**, 96010J (2015).
[7]B. Alpert, M. Balata, D. Bennett, M. Biasotti, C. Boragno, C. Brofferio, V. Ceriale, D. Corsini, P. K. Day, M. De Gerone *et al.*, Eur. Phys. J. C **75**, 112 (2015).
[8]H. Tatsuno, W. B. Doriese, D. A. Bennett, C. Curceanu, J. W. Fowler, J. Gard, F. P. Gustafsson, T. Hashimoto, R. S. Hayano, J. P. Hays-Wehle *et al.*, J. Low Temp. Phys. **184**, 930 (2016).
[9]J. N. Ullom, W. B. Doriese, D. A. Fischer, J. W. Fowler, G. C. Hilton, C. Jaye, C. D. Reintsema, D. S. Swetz, and D. R. Schmidt, Synchrotron Radiat. News **27**, 24 (2014).
[10]J. N. Ullom and D. A. Bennett, Supercond. Sci. Technol. **28**, 084003 (2015).
[11]W. B. Doriese, K. M. Morgan, D. A. Bennett, E. V. Denison, C. P. Fitzgerald, J. W. Fowler, J. D. Gard, J. P. Hays-Wehle, G. C. Hilton *et al.*, J. Low Temp. Phys. **184**, 389 (2016).

[12]J. Chervenak, K. Irwin, E. Grossman, J. Martinis, C. Reintsema, and M. Huber, Appl. Phys. Lett. **74**, 4043 (1999).
[13]L. Gottardi, J. van de Kuur, S. Bandler, M. Bruijn, P. de Korte, J. R. Gao, R. den Hartog, R. A. Hijmering, H. Hoevers *et al.*, IEEE Trans. Appl. Supercond. **21**, 272 (2011).
[14]J. A. B. Mates, G. C. Hilton, K. D. Irwin, L. R. Vale, and K. W. Lehnert, Appl. Phys. Lett. **92**, 023514 (2008).
[15]O. Noroozian, J. A. B. Mates, D. A. Bennett, J. A. Brevik, J. W. Fowler, J. Gao, G. C. Hilton, R. D. Horansky, K. D. Irwin, Z. Kang *et al.*, Appl. Phys. Lett. **103**, 202602 (2013).
[16]G. M. Stiehl, W. B. Doriese, J. W. Fowler *et al.*, Appl. Phys. Lett. **100**, 072601 (2012).
[17]J. L. Walsh, Am. J. Math. **45**, 5 (1923).
[18]K. D. Irwin, M. D. Niemack, J. Beyer, H. M. Cho, W. B. Doriese, G. C. Hilton, C. D. Reintsema, D. R. Schmidt, J. N. Ullom, and L. R. Vale, Supercond. Sci. Technol. **23**, 034004 (2010).
[19]M. D. Niemack, J. Beyer, H. M. Cho, W. B. Doriese, G. C. Hilton, K. D. Irwin, C. D. Reintsema, D. R. Schmidt, J. N. Ullom, and L. R. Vale, Appl. Phys. Lett. **96**, 163509 (2010).
[20]H. Zappe, IEEE Trans. Magn. **13**, 41 (1977).
[21]J. W. Fowler, W. B. Doriese, G. Hilton, K. Irwin, D. Schmidt, G. Stiehl, D. Swetz, J. N. Ullom, and L. Vale, J. Low Temp. Phys. **167**, 713 (2012).
[22]D. S. Swetz, D. A. Bennett, K. D. Irwin, D. R. Schmidt, and J. N. Ullom, Appl. Phys. Lett. **101**, 242603 (2012).
[23]G. Holzer, M. Fritsch, M. Deutsch, J. Hartwig, and E. Forster, Phys. Rev. A **56**, 4554 (1997).
[24]W. Doriese, J. Adams, G. Hilton, K. D. Irwin, C. Kilbourne, F. Schima, and J. Ullom, AIP Conf. Proc. **1185**, 450 (2009).
[25]W. B. Doriese, B. K. Alpert, J. W. Fowler, G. C. Hilton, A. S. Hojem, K. D. Irwin, C. D. Reintsema, D. R. Schmidt, G. M. Stiehl *et al.*, J. Low Temp. Phys. **167**, 595 (2012).
[26]W. B. Doriese, J. A. Beall, W. D. Duncan, L. Ferreira, G. C. Hilton, K. D. Irwin, C. D. Reintsema, J. N. Ullom *et al.*, Nucl. Instrum. Methods Phys. Res., Sect. A **559**, 808 (2006).
[27]L. M. Avila, K. Silverman, D. Bennett, C. Cromer, M. Dowell, J. Fowler, W. Doriese, G. O'Neil, D. Swetz *et al.*, in *CLEO: QELS* (Optical Society of America, 2013), p. QTh4D–7.
[28]J. Ullom, M. Dowell, J. Fowler, L. Miaja, G. O'Neil, K. Silverman, D. Swetz, D. Sagar *et al.*, in *CLEO: Applications and Technology* (Optical Society of America, 2014), p. AW1P–3.
[29]J. Fowler, B. Alpert, W. Doriese, Y.-I. Joe, G. O'Neil, J. Ullom, and D. Swetz, J. Low Temp. Phys. **184**, 374 (2016).
[30]J. Yoon, J. Clarke, J. Gildemeister, A. Lee, M. Myers, P. Richards, and J. Skidmore, Appl. Phys. Lett. **78**, 371 (2001).